Preprints of the 21st IFAC World Congress (Virtual)
Berlin, Germany, July 12-17, 2020

Model Predictive Energy Control Including Mechanical Fatigue Life of a Two-Motor Multi-Speed Electric Vehicle

Y. Tao* D. Schoeneberger* S. Rinderknecht*
B. Morhard D. Schweigert** M. Gerlach*** U. Obernolte******

**Institute for Mechatronic Systems, Technical University of Darmstadt, Darmstadt 64287, Germany*
***Gear Research Centre, Technical University of Munich, Munich 85748, Germany*
**** Institute for Drive Systems and Power Electronics, Leibniz University of Hannover, Hannover 30167, Germany*
*****Lenze SE, Hameln 31763, Germany*

Abstract: Over the last three decades, energy management strategies considering minimum energy consumption have been extensively studied in the field of automotive engineering. On the contrary, the fatigue life of mechanical parts in powertrains is rarely considered. This paper addresses a Real-time-oriented Multi-Objective Energy Management Strategy aimed at both the energy consumption and the fatigue life of mechanical parts in the powertrain of a Two-Motor Multi-Speed Battery Electric Vehicle (BEV). This strategy is based on Model Predictive Control (MPC), while Dynamic Programming (DP) is embedded to solve the non-linear optimal control problem in the prediction horizon. The online simulation results show that this MPC-based strategy prolongs the service life of the powertrain with a minor sacrifice in energy consumption, and that this strategy achieves a sub-optimal result close to the offline optimal result from DP. Moreover, the result from MPC-based strategy approaches the optimal result with prolonging prediction horizon.

Keywords: Automotive Control; Battery Electric Vehicle; Powertrain; Multi-Objective Energy Management Strategy; Optimal Control; Fatigue Life; Service Life; Model Predictive Control; Real-Time Control.

1. INTRODUCTION

Under the ascending pressure from the emission and fuel consumption regulation (EU Parliament (2019)), vehicle electrification has been receiving continuously uprising attention both in market and in academia. Being completely electrified, Battery Electric Vehicles (BEV) generate zero operational emissions compared with conventional vehicles and have more simple propulsion systems compared with Hybrid Electric Vehicles (HEV). The problem of high pricing, one of the main obstacles between BEVs and consumers, is gradually eased by declining battery prices (Wolfram et al. (2016)). Therefore, BEVs are playing a stronger role in the market: BEVs took 31.3 % and 44.7 % of new passenger car sales in 2018 and the first 9 months of 2019 respectively (Grundhoff (2019)); the market share of BEV in a Belgian city is forecasted to reach 15 % by 2030 (Lebeau et al. (2012)).

Another main bottleneck keeping BEVs from popular adoption is the low energy density of Lithium-ion battery compared with standard fuel (Manzetti et al. (2015)). Thus, efficiency of the whole powertrain plays an important role to extend the range of BEVs. A pioneer Project 'Speed4E' introduced an innovative Two-Motor Multi-Speed powertrain (Mileti et al. (2019)). Compared with normal BEV powertrain topologies shown in Fig. 1 (a) and (b) (Ivanov et al. (2015)), the Speed4E powertrain (c) consists of two electric motors and corresponding sub-transmissions, which enables a power-split between the motors as well as a gear selection in favour of higher overall efficiency of the powertrain. Besides, the combination of hyper-high-speed electric motors (maximum motor speed 50000 rpm) and high gear ratio meets the output torque requirement and has the advantage of downsized and lightweight electric motors.

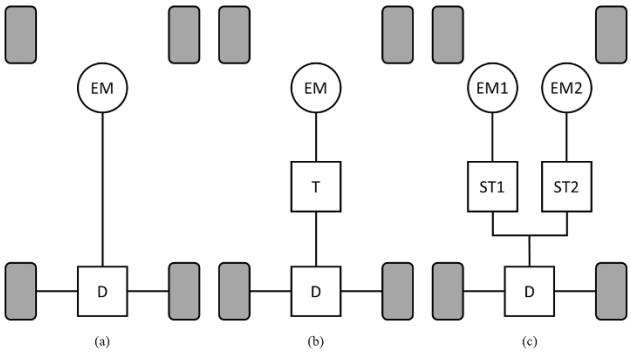

Fig. 1. BEV powertrain topologies. EM: Electric Motor, T: Transmission, D: Final Drive, ST: Sub-Transmission. Variants: (a) Direct Central; (b) Central with Transmission; (c) Speed4E powertrain with two electric motors and corresponding sub-transmission.

Given this Speed4E powertrain, certain energy management strategies are investigated. Shortly after rule-based strategies (Opila et al. (2000)) were proposed, the focus of this area shifted to optimal control theory, viewing the energy management problem as an Optimal Control Problem (OCP). Dynamic Programming (DP), a direct method delivering a global optimum, has received attention since then (Brahma et al. (2000)). In the same period, Equivalent Consumption Minimization Strategy (ECMS), an application and a

simplification of an indirect method, Pontryagin's Maximum Principle (PMP), was proposed (Paganelli et al. (2002)). Though simplified, ECMS still achieved nearly identical result as PMP (Kim et al. (2011)).

In order to achieve better real-time control performance, Model Predictive Control (MPC) was applied in HEV energy management strategies; a review of these applications was written by Huang (Huang et al. (2017)). MPC solves an OCP over a receding horizon and apply the control policy in the control horizon, which results in a suboptimal control. Certain MPC algorithms were studied and achieved 96% of the optimality from DP under the examined drive cycle (H. Banvait et al. (2014)).

Though sharing same methods from optimal control theory, developing energy management strategies for BEV differs in certain area. First of all, the strategy aims at minimum fuel consumption in the case of HEV and minimum battery discharge in the case of BEV; Secondly, though the time directive of SOC depends both on the battery power and itself, the battery power is independent of SOC; Thirdly, the total power request must be met by the battery no matter the SOC condition. Therefore, SOC no longer exists in the OCP and the cost function is transformed to battery power for BEV.

Plenty of energy management strategies were developed from DP, ECMS, MPC and so forth. However, these strategies mainly considered energy consumption. Although occasional considerations of shift frequency (Yuan et al. (2013)), emission (Pisu et al. (2007)), and battery aging (Li et al. (2018)) also exist, the fatigue life of the mechanical parts in the powertrain is neglected. The downside is that an energy consumption oriented control strategy would split the power between power sources as well as select the gear in a fixed manner given fixed drive cycle and drive routine, which leads to higher accumulated fatigue of certain mechanical parts and therefore an uneven distribution of accumulated fatigue in the powertrain. In the best case, these parts are to be replaced after they meet the fatigue limit. In the worst case, the whole system is to be replaced. A strategy aimed at both energy consumption and fatigue life of mechanical parts could reduce the economical and ecological cost and waste in this process. Besides, all mechanical parts are designed to meet certain fatigue life requirements. A control strategy aimed also at fatigue life of mechanical parts can intelligently arrange loads on different gears and power sources and therefore has the potential benefit of vehicle lightweighting through lowering these fatigue life requirements.

This paper proposes a real-time-control-oriented energy management strategy considering both the energy consumption and the fatigue life of the mechanical parts in the powertrain of the Speed4E vehicle. It can also be applied to other powertrain topologies if the vehicle and the powertrain models are modified. This strategy is based on a DP-embedded MPC algorithm and a simulation study is conducted. Because computational cost is crucial to real-time application, the influence from the length of the prediction horizon to simulation results and computation durations is investigated.

This paper is organized as follows. The architecture of the studied BEV and the model of mechanical fatigue life are presented in Section II. The multi-objective OCP is formulated and the algorithms to solve this optimal control problem with MPC are presented in Section III. In Section IV, simulation results of the control strategy developed from MPC are compared with the results from DP. The influence of prediction horizon to the results and computational cost is studied in Section IV. Latter comes conclusion as Section V.

2. VEHICLE AND MECHANICAL FATIGUE LIFE MODELS

2.1 Vehicle Model

This study considers the prototype BEV designed in the project "Speed4E". As discussed in the introduction, its powertrain consists of two electric motors, two corresponding sub-transmissions and a final drive. Electric Motor 1 (EM1) is connected with the fixed gear sub-transmission 1 (ST1), a planetary gear set, while Electric Motor 2 (EM2) is connected with sub-transmission 2 (ST2), a 3-stage 2-speed helical gear set. As the two EMs as well as STs work independently from each other, the output torque can be split between the two sub-powertrains and the ST2 can be shifted to 1st gear with high gear ratio in favour of high output torque for acceleration or 2nd gear with low gear ratio in favour of the operational efficiency of EM2. The schematic representation Speed4E powertrain is presented in Figure 2. The vehicle configurations are reported in Table 1. The speed-torque relation of the powertrain is described in (3).

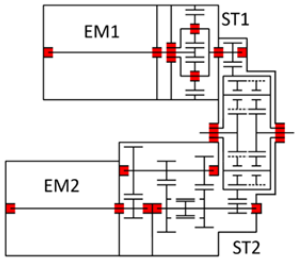

Fig. 2. Schematic representation of the Speed4E powertrain (Mileti et al. (2019))

Table 1. Basic Vehicle Information

Fronted area	2.38 m²
Aerodynamic coefficiency	0.294
Rolling coefficient	Velocity dependent curve
Electric Motor 1	Induction motor Rated speed: 20000 rpm Rated torque: 28 Nm Maximum speed: 30000 rpm Maximum torque: 60 Nm

Electric Motor 2	Permanent magnet motor Rated speed: 26000 rpm Rated torque: 27 Nm Maximum speed: 50000rpm Maximum torque: 43 Nm
Sub-Transmission 1	Fixed gear ratio: 26.4
Sub-Transmission 2	1st gear ratio: 36 2nd gear ratio: 20

The vehicle dynamics are calculated as in

$$P_{req}(t) = \Big(e_i m a_{veh}(t) + c_{roll}(t) m g \cos\big(\theta(t)\big) + \frac{1}{2} c_{aero} \cdot \rho_{air} A_f v_{veh}^2(t) + m g \sin\big(\theta(t)\big) \Big) v_{veh}(t), \quad (1)$$

where P_{req} is the requested power; e_i is the mass factor, which is an effect of rotating components in the powertrain; m is the total mass of the vehicle; a_{veh} is the vehicle acceleration; rolling resistance is calculated according to coefficient c_{roll} and gravity force normal to the ground $mg\cos\theta$; aerodynamic resistance is calculated according to coefficient c_{aero}, density of the air ρ_{air}, fronted aero A_f and the vehicle velocity v_{veh}; $mg\sin\theta$ is the gravity force parallel to the ground.

The requested power is balanced by the output power of the powertrain as in

$$P_{req}(t) = M_{req}(t) \cdot \omega_{wheel}(t), \quad (2)$$

$$M_{req}(t) = M_{EM1}(t) \cdot i_{ST1} \cdot \eta_{ST1}^{l}(\omega_{EM1}, M_{EM1}) + M_{EM2}(t) \cdot i_{ST2}(G) \cdot \eta_{ST2}^{l}(\omega_{EM2}, M_{EM2}, G), \quad (3)$$

where M_{req} is the requested output torque of the powertrain; M_{EM} is the output torque of an electric motor; ω is the rotational speed; i is the gear ratio (fixed for ST1 and depending on gear selection for ST2); η is the efficiency (depending on the speed and the torque of EM1 for ST1 and on the speed and the torque of EM2 as well as the gear selection G for ST2); l is -1 when motoring and 1 when recuperating.

All the power is provided by the battery as in

$$P_{batt}(t) = P_{EM1}(t) \cdot \eta_{EM1}^{l}(\omega_{EM1}, M_{EM1}) \cdot \eta_{PE1}^{l}(\omega_{EM1}, M_{EM1}) + P_{EM2}(t) \cdot \eta_{EM2}^{l}(\omega_{EM2}, M_{EM2}) \cdot \eta_{PE2}^{l}(\omega_{EM2}, M_{EM2}), \quad (4)$$

where P_{batt} is the battery electric power; η_{EM} is the efficiency of the electric motor; η_{PE} is the efficiency of the power electronic.

The efficiency of power electronics, electric motors and transmissions are modelled as corresponding maps based on the simulation results from project partners Lenze, IAL-AS University of Hannover and FZG Technical University of Munich respectively.

2.2 Fatigue Life Model of Mechanical Parts

This part presents the method used in this paper to calculate certain mechanical parts' fatigue life under operational condition. Gear sets and their tooth flank pitting are chosen as the object of the fatigue life model in this study. However, fatigue life of other mechanical parts in the powertrain, for instance bearings, can also be modelled (Tong et al. (2017)) and implemented.

2.2.1 Miner Rule

Miner rule is the basis of almost all known fatigue life calculation methods for cyclically loaded components characterized by a nominal stress, especially in the automotive field (Bertsche (2008), 325–329). The fundamental ideas and assumptions are: 1) the component absorbs work during fatigue process, and the ratio of already absorbed work w to the maximum absorbable work W is the measure of the fatigue D. This can be converted to the ratio of already happened cycle number n to the maximum permissible cycle number N under certain cycle stress S from Woehler curve, also known as S-N curve; 2) every cycle under the same stress condition causes same fatigue; 3) all partial fatigues D_i can be linearly accumulated to calculate total fatigue D; 4) a failure occurs when total fatigue reaches 1. These statements can be represented by (5) and (6), in which k means the number of cycle stress levels. The S-N curves used in this study are based on the calculation from FZG Technical University of Munich.

$$D = \frac{w}{W} = \frac{n}{N} \quad (5)$$

$$D = \sum_{i=1}^{k} D_i = \sum_{i=1}^{k} \frac{w_i}{W} = \sum_{i=1}^{k} \frac{n_i}{N_i} \quad (6)$$

2.2.2 Nominal Stress on Gear Flank

As stated in the beginning of this chapter, this study consider the tooth flank pitting as failure in this study and therefore need to calculate the stress on the flank. In this study, the Hertzian contact pressure (Niemann et al. (2003)) based method from DIN 3990 (Deutsches Institut für Normung E.V. (DIN)) is used and presented as in

$$\sigma_H = Z_H \cdot Z_E \cdot Z_\varepsilon \cdot Z_\beta \cdot Z_{1,2} \sqrt{\frac{2000 \cdot T_{\text{input}}}{d_1 \cdot b} \cdot \frac{d_1 + d_2}{d_1 \cdot d_2} \cdot K_v \cdot K_{H\beta} \cdot K_{H\alpha}}, \quad (7)$$

where σ_H is Hertzian pressure; Z_H is zone factor; Z_E is elasticity factor; Z_ε is contact ratio factor; Z_β is helix angle factor; $Z_{1,2}$ is tooth contact factor; 1 for pinion, 2 for gear; T_{input} is input torque to the gear set; d is pitch circle diameter; K_v is dynamic factor; $K_{H\beta}$ is face load distribution factor for contact pressure; $K_{H\alpha}$ is transverse factor for contact pressure. A more detailed description and how to pick these factors can be found in DIN3990.

2.2.3 Fatigue Life of Mechanical Parts and Mechanical Service Life of the Powertrain

The fatigue life F is defined as in

$$F = \frac{1}{D} \cdot L_{cycle}, \quad (8)$$

where L_{cycle} is the distance of the tested drive cycle or the driving distance in real world. The mechanical part with the shortest fatigue life determines the mechanical service life of the powertrain.

3. FORMULATION AND SOLUTION OF OPTIMAL CONTROL PROBLEM

3.1 Formulation of the Optimal Control Problem

The OCP is formulated here in a discrete form with a time index k. The optimization horizon $[t_0,t_f]$ is evenly discretised to N steps with 1 second time step. The system state $x(k) = (x_1(k), x_2(k))^T = (P_{batt}(k), \omega_{EM1}(k))^T$ evolves as (9) under constraints of (10), where f is transformed from (1), (2), (3) and (4), which describe the dynamics of the vehicle and the powertrain under certain requested power (P_{req}). The torque of EM1 and the gear selection are chosen as the control ($u(k) = (u_1(k), u_2(k))^T = (M_{EM1}(k), G(k))^T$).

$$x(k+1) = f\big(x(k), u(k)\big) \quad \forall k \in \{0,1,2 \dots k, k+1 \dots N-1, N\} \quad (9)$$

$$s.t. \begin{cases} P_{batt,min} \le x_1(k) \le P_{batt,max} \\ \omega_{EM1,min} \le x_2(k) \le \omega_{EM1,max} \\ M_{EM1,min} \le M_{EM1}\big(x(k),u(k)\big) \le M_{EM1,max} \\ \omega_{EM2,min} \le \omega_{EM2}\big(x(k),u(k)\big) \le \omega_{EM2,max} \\ M_{EM1,min} \le u_1(k) \le M_{EM1,max} \\ u_2(k) \in \{0,1,2\} \end{cases} \quad (10)$$

Determined by the state at 0 and the policy π, a sequence of controls described in (12), the cost function (11) consists of two parts and a fatigue weight factor β. Battery electric power in (13) represents the energy consumption. Function (14) is the squared deviation of the fatigue of the pinion of stage 1 in ST1 and the fatigue of the sun gear of stage 1 in ST2. To make the sentences more compact, we call them fatigue of ST1 and ST2. Minimizing the squared deviation means balancing the fatigue of ST1 and ST2 so that the mechanical service life of the powertrain is prolonged. Solving an OCP means finding the value function $J^*\big(x(0)\big)$ described as in (15) and corresponding optimal control policy π^*.

$$J(x(0),\pi) = \sum_{k=0}^{N} \Big(g_{energy}\big(x(k),u(k)\big) + \beta g_{fatigue}\big(x(k),u(k)\big) \Big) \quad (11)$$

$$\pi = \{u(0), u(1) \dots u(N)\} \quad (12)$$

$$g_{energy}\big(x(k),u(k)\big) = P_{batt}\big(x(k),u(k)\big) \quad (13)$$

$$g_{fatigue}\big(x(k),u(k)\big) = \Big(D_{sungear,ST1}\big(x(k),u(k)\big) - D_{pinion,ST2}\big(x(k),u(k)\big) \Big)^2 \quad (14)$$

$$J^*\big(x(0)\big) = \min_{\pi}\{J(x(0),\pi)\} \quad (15)$$

3.2 Dynamic Programming Solution

Bellman's equation is applied to the OCP as in (16) with the final stage condition $J^*\big(x(N)\big) = 0$, and thereafter the optimal policy π^* in (17) is determined.

$$J^*\big(x(k)\big) = \min_u \{ g_{energy}\big(x(k),u(k)\big) + \beta g_{fatigue}\big(x(k),u(k)\big) + J^*\big(f\big(x(k),u(k)\big)\big) \} \quad (16)$$

$$\pi^* = \{u^*(0), u^*(1) \dots u^*(N)\} \quad (17)$$

3.3 Application of Model Predictive Control

Fig. 3(a) shows the flowchart of the MPC algorithm with a time step of 1 second in this study. At every time step j, the future driver torque request is generated according to the exponential decreasing function (Borhan et al. (2009)) described as in (18) and (19), determining the system state in the prediction horizon (m_p red circled line in Fig. 3 (b)). The choice of an inconsistent T_d is based on the observation from the daily life that the higher the requested torque, the shorter the duration of the request. The DP algorithm described in 3.2 is embedded to determine the optimal policy π^* in the prediction horizon (light blue steps in Fig. 3(b)). π^* is applied

in the control horizon (m_c) following the past control, the darker blue steps. This procedure repeats until the end of the total simulation horizon N.

$$M_{\mathrm{req}}(j+i) = M_{\mathrm{req}}(j)\exp\left(-\frac{i}{T_d}\right) \qquad i = 1,2 \ldots m_p \tag{18}$$

$$T_d = \begin{cases} 0.1 & 1000 \le M_{\mathrm{req}}(j) \\ 1 & 100 \le M_{\mathrm{req}}(j) < 1000 \\ 0.1 & M_{\mathrm{req}}(j) < 100 \end{cases} \tag{19}$$

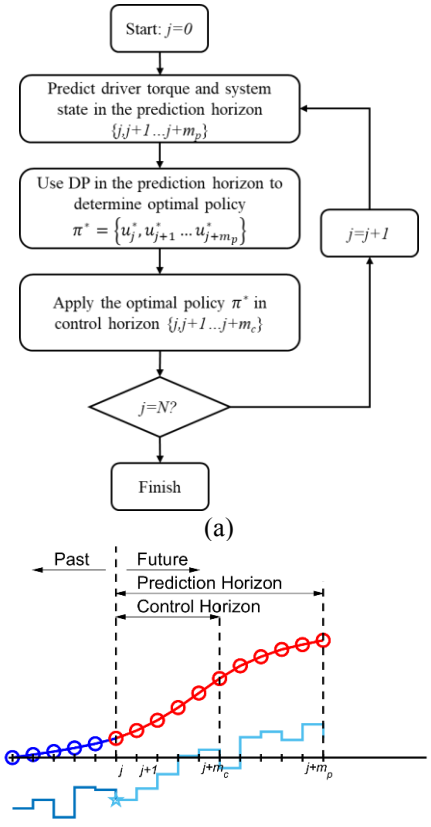

Fig. 3. Flowchart and schematic of MPC algorithm in this study

4. SIMULATION RESULTS

4.1 Simulation Results with DP

DP is used to generate a global optimal control strategy given Worldwide Harmonized Light Vehicle Test Procedure (WLTP) drive cycle as a priori. The simulation results are shown in Fig. 4. Every green circle represents the squared deviation of fatigue and the energy consumption of one WLTP drive cycle with respective weight factor as in (20), where the subscript p is the index of the weight factors and the test cases. The red and the blue circle vertical to each green circle represent the fatigue of ST1 and ST2 after one WLTP drive cycle regarding the same weight factor as the green circle.

$$\beta_p = 10^q \qquad q = \begin{cases} 2p & 0 \le p \le 7 \\ 0.5p + 11 & 7 < p \le 19 \end{cases} \tag{20}$$

Due to small order of magnitude of the fatigue part in the cost function (11), no obvious change takes place before the weight factor reaches β_{11}. The nonlinear relation between the index of weight factor p and order q in (20) is intended to spare Fig. 4 from crowded data points between β_1 and β_{11}. When β stays at a low level, the accumulated fatigue of ST1 is more than two times of ST2, resulting half of the fatigue life. The reason is that the sub-powertrain 1, the combination of EM1 and ST1, operates with a higher efficiency in most of the operation states in WLTP. Fig. 4 shows that a rising weight factor β diminishes the squared deviation of fatigue. The fatigue of ST1 reaches its minimum at β_{14} resulting its longest fatigue life and the longest service life of the powertrain, which increases by 13.6 % compared with the one with β_1 (β_1: 1.87x10^5 km and β_{14}: 2.15x10^5 km). Meanwhile, only 1.7% more energy is consumed (β_1: 13.36 kWh/100 km and β_{14}: 13.59 kWh/100 km).

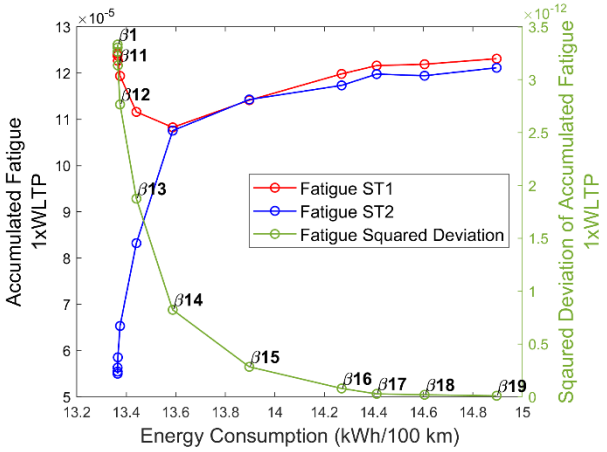

Fig. 4. DP control strategy simulation results with different weight factors β

Fig. 5 and Fig. 6 illustrate the gear selection and the resulting load spectra, accumulated cycle numbers regarding different stress levels on S-N curve diagram (Naunheimer et al. (2007), 250–254), of ST1 and ST2 with different weight factors β. Comparing Fig. 5 (b) to Fig. 5 (a), a higher weight factor shrinks ST2-neutral-gear to vehicle velocities under 60 km/h and low battery power in favour of balanced fatigue. Thus, the loaded cycle numbers of ST1 decreased between 0.08 and 0.25 normalized stress (Fig. 6 (a)); the load spectrum of ST2 extend to 0.08 normalized stress (Fig. 6 (b)); the highest stress level of ST1 and ST2 both decrease.

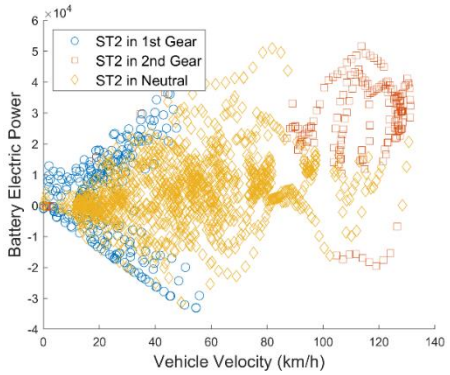

(a) Gear selection with β_1

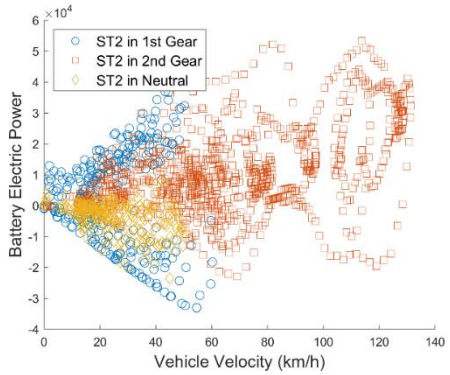

(b) Gear selection with β_{14}

Fig. 5. Gear selection with different weight factors

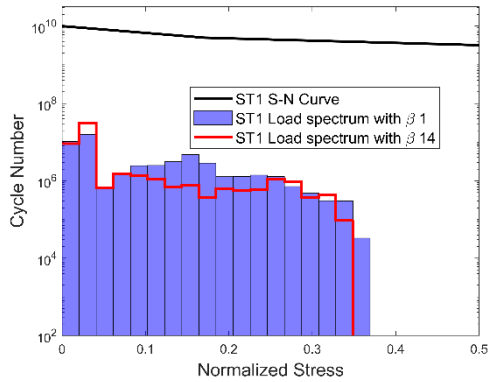

(a) ST1 load spectrum after one cycle of WLTP

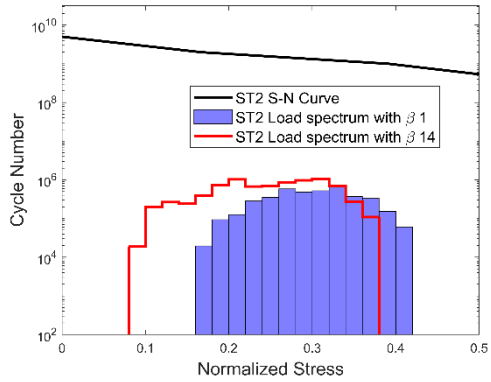

(b) ST2 load spectrum after one cycle of WLTP

Fig. 6. Load spectrum with different weight factors

4.2 Online Simulation Results with MPC

4.2.1 Online Simulation Results compared with Offline Results from DP

Fig. 7 shows an overall comparison between MPC online simulation results and DP offline simulation results with same weight factors. Because the MPC algorithm does not consider the drive cycle a priori, it cannot exploit all the information and therefore reaches suboptimal results. A comparison of energy consumption and service life of the powertrain is presented in Table 2. When the control strategy neglects fatigue, the energy consumption of MPC is merely 0.3% more than that of DP. When it shares β_{14} as DP, MPC consumes 0.4% more energy and causes the powertrain service life to be 1.4% less.

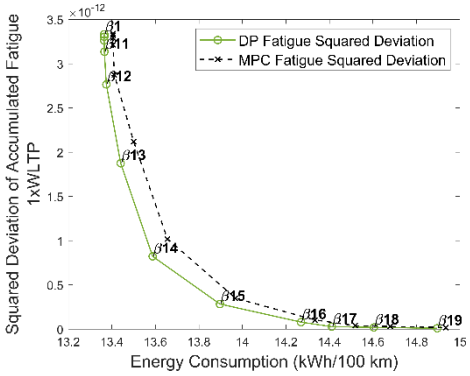

Fig. 7. MPC online simulation results. m_p=5, m_c=1.

Table 2. MPC (m_p=5, m_c=1) and DP Simulation Results Comparison

	β_1		β_{14}	
	DP	MPC	DP	MPC
Energy consumption (kWh/100km)	13.36	13.40 (+0.3 %)	13.59	13.65 (+0.4 %)
Powertrain service life under WLTP (x10^5 km)	1.87	1.88 (+0.5 %)	2.15	2.12 (-1.4 %)

4.2.2 Simulation Results and Computation Duration of MPC with different Prediction Horizon

Fig. 8 illustrates the influence of the prediction horizon's length to the simulation results, whose exact numbers are presented in Table 3 (β_{14} as the study case; m_p sequentially increases from 5 to 15). The MPC online simulation results approach the optimal offline result from DP with prolonging prediction horizon. Increasing the prediction horizon from 5 to 9 causes a decrement of energy consumption 4 times more than the decrement through increasing prediction horizon

from 9 to 15, while it's a 1.5 times in the case of the powertrain service life.

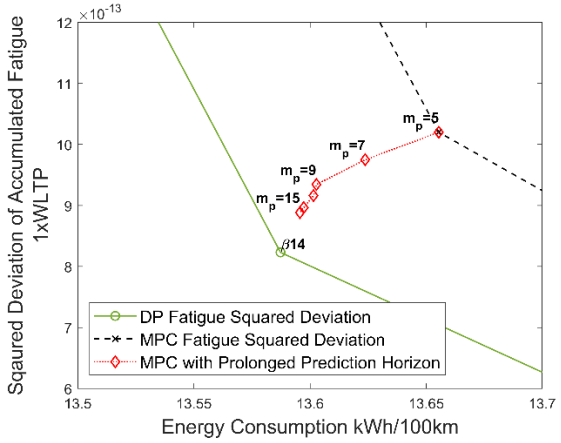

Fig. 8. MPC simulation results with prolonged prediction horizon

Table 3. MPC Simulation Results with Prolonged Prediction Horizon

	DP	MPC, m_p=5	MPC, m_p=9	MPC, m_p=15
Energy consumption (kWh/100km)	13.587	13.652 (+0.4 %)	13.603 (+0.1 %)	13.596 (+0.1 %)
Powertrain service life under WLTP (x10^5 km)	2.148	2.119 (-1.4 %)	2.129 (-0.9 %)	2.133 (-0.7 %)

Fig. 9 shows the computation duration for one WLTP of the cases presented in Fig. 8. Linear square regression (LSR) is applied to these data points and a clear linear correlation can be noticed. The reason is that DP is embedded to determine the optimal policy in the prediction horizon (subsection 3.3), while DP's computational complexity grows linearly with recursion steps (equation (15)).

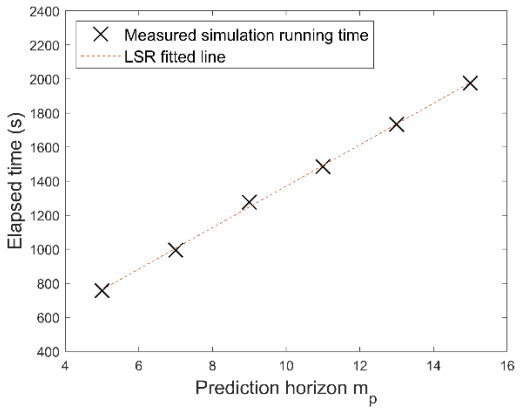

Fig. 9. Computation duration of MPC algorithm for one WLTP cycle. Computer configuration: i5-8600K, 3.6 GHz.

Prolonging prediction horizon length causes different improvement rates of the simulation results but linear growth of the computation durations. Therefore, we choose m_p=9, where the decreasing of energy consumption in Fig. 8 softened, for the future test of real-time control. This mindset is similar to the elbow method in clustering (Kodinariya et al. (2013)). It achieves a simulation duration 0.7 time of the WLTP cycle duration and delivers a result coinciding the offline optimal result with DP (Table 3). Thus, such a DP-embedded-MPC algorithm has the potential to serve as real-time controller and deliver close to optimal result.

5. CONCLUSION

This paper firstly proposes a non-linear multi-objective OCP considering the energy consumption and the fatigue life of mechanical parts in the powertrain as well as shows the integration of the mechanical fatigue life model into the Speed4E vehicle model. Secondly, DP-based energy management strategy regarding the proposed OCP prolongs the powertrain service life with subtle sacrifice in the energy consumption. With a weight factor of β_{14}, the service life is prolonged by 13.6% while the EV consumes 1.7% more electric energy. Thirdly, a DP-embedded-MPC-based strategy is presented, achieving close to optimal results from DP. Moreover, the investigation of the prediction horizon length shows its linear correlation to the simulation duration and that the MPC-based strategy approaches the optimal result with prolonging prediction horizon. We choose a prediction horizon of 9 steps as a compromise.

REFERENCES

Bertsche, B. (2008). *Reliability in automotive and mechanical engineering: Determination of component and system reliability*. *VDI-Buch*: Springer.

Borhan, H. A., Vahidi, A., Phillips, A. M., Kuang, M. L., & Kolmanovsky, I. V. (2009). Predictive energy management of a power-split hybrid electric vehicle, 3970–3976.

Brahma, A., Guezennec, Y., & Rizzoni, G. [G.] (2000). Optimal energy management in series hybrid electric vehicles. *American Control Conference*, 60-64 vol.1.

Deutsches Institut für Normung E.V. *Tragfähigkeitsberechnung von Stirnrädern*. (3990-6).

EU Parliament (2019). REGULATION (EU) 2019/ 631 OF THE EUROPEAN PARLIAMENT AND OF THE COUNCIL - of 17 April 2019 - setting CO2 emission performance standards for new passenger cars and for

new light commercial vehicles, and repealing Regulations (EC) No 443 / 2009 and (EU) No 510 / 2011: setting CO2 emission performance standards for new passenger cars and for new light commercial vehicles, and repealing Regulations (EC) No 443/2009 and (EU) No 510/2011. *Official Journal of European Union*.

Grundhoff, S. (2019). Norwegen will Elektroanreize bis 2021 beibehalten. Retrieved from https://www.automobil-produktion.de/hersteller/wirtschaft/norwegen-will-elektroanreize-bis-2021-beibehalten-259.html

H. Banvait, J. Hu, & Y. Chen (2014). Energy management control of plug-in hybrid electric vehicle using hybrid dynamical systems. *IEEE TRANSACTIONS ON INTELLIGENT TRANSPORTATION SYSTEMS,*.

Huang, Y., Wang, H., Khajepour, A., He, H., & Ji, J. (2017). Model predictive control power management strategies for HEVs: A review. *Journal of Power Sources*, *341*, 91–106.

Ivanov, V., Savitski, D., & Shyrokau, B. (2015). A Survey of Traction Control and Antilock Braking Systems of Full Electric Vehicles With Individually Controlled Electric Motors. *IEEE Transactions on Vehicular Technology*, *64*(9), 3878–3896.

Kim, N., Cha, S., & Peng, H. (2011). Optimal Control of Hybrid Electric Vehicles Based on Pontryagin's Minimum Principle. *IEEE Transactions on Control Systems Technology*, *19*(5), 1279–1287.

Kodinariya, T., & Makwana, P. (2013). Review on determining number of cluster in K-Means Clustering. *International Journal of Advance Research in Computer Science and Management Studies*, 90–95.

Lebeau, K., van Mierlo, J., Lebeau, P., Mairesse, O., & Macharis, C. (2012). The market potential for plug-in hybrid and battery electric vehicles in Flanders: A choice-based conjoint analysis. *Transportation Research Part D: Transport and Environment*, *17*(8), 592–597.

Li, J., Huber, T., & Beidl, C. (2018). Predictive Multi-Objective Operation Strategy Considering Battery Cycle Aging for Hybrid Electric Vehicles. *SAE International Journal of Alternative Powertrains*, *7*(3), 217–232.

Manzetti et al. (2015). Electric vehicle battery technologies: From present state to future systems. *Renewable and Sustainable Energy Reviews*, *51*, 1004–1012.

Mileti et al. (2019). Speed4E Hyper-High-Speed Driveline and Gearbox for BEVs. *13th International CTI Symposium 'Automotive Drivetrains, Intelligent, Electrified'*.

Naunheimer, H., Bertsche, B., Lechner, G., Ryborz, J., & Novak, W. (2007). *Fahrzeuggetriebe: Grundlagen, Auswahl, Auslegung und Konstruktion* (2., bearb. und erw. Aufl.). *VDI-Buch*. Berlin: Springer.

Niemann, G., & Winter, H. (2003). *Getriebe allgemein, Zahnradgetriebe - Grundlagen, Stirnradgetriebe* (2., völlig neubearb. Aufl., 2. berichtigter Nachdr., korrigierter Nachdr). *Maschinenelemente: / G. Niemann; H. Winter ; Bd. 2*. Berlin: Springer.

Opila et al. (2000). FUNDAMENTAL STRUCTURAL LIMITATIONS OF AN INDUSTRIAL ENERGY. *IEEUASME Transactions on Mechatronics*. (5), 58–72.

Paganelli, G., Delprat, S., Guerra, T. M., Rimaux, J., & Santin, J. J. (2002). Equivalent consumption minimization strategy for parallel hybrid powertrains. *Vehicular Technology Conference*, 2076–2081.

Pisu, P., & Rizzoni, G. [Giorgio] (2007). A Comparative Study Of Supervisory Control Strategies for Hybrid Electric Vehicles. *IEEE Transactions on Control Systems Technology*, *15*(3), 506–518.

Tong, V.-C., Kwon, S.-W., & Hong, S.-W. (2017). Fatigue life of cylindrical roller bearings. *Proceedings of the Institution of Mechanical Engineers, Part J: Journal of Engineering Tribology*, *231*(5), 623–636.

Wolfram, P., & Lutsey, N. (2016). Electric vehicles: Literature review of technology costs and carbon emissions. *INTERNATIONAL COUNCIL ON CLEAN TRANSPORTATION*.

Yuan, Z., Teng, L., Fengchun, S., & Peng, H. (2013). Comparative Study of Dynamic Programming and Pontryagin's Minimum Principle on Energy Management for a Parallel Hybrid Electric Vehicle. *Energies*, *6*(4), 2305–2318.